



Digital Rock Samples Porosity Analysis by OTSU Thresholding Technique Using MATLAB

Yahya J. Tawfeeq and Jalal A. Al-Sudani

Petroleum Engineering Department, College of Engineering, University of Baghdad, Baghdad, Iraq

Abstract

Porosity plays an essential role in petroleum engineering. It controls fluid storage in aquifers, connectivity of the pore structure control fluid flow through reservoir formations. To quantify the relationships between porosity, storage, transport and rock properties, however, the pore structure must be measured and quantitatively described. Porosity estimation of digital image utilizing image processing essential for the reservoir rock analysis since the sample 2D porosity briefly described. The regular procedure utilizes the binarization process, which uses the pixel value threshold to convert the color and grayscale images to binary images. The idea is to accommodate the blue regions entirely with pores and transform it to white in resulting binary image. This paper presents the possibilities of using image processing for determining digital 2D rock samples porosity in carbonate reservoir rocks. MATLAB code created which automatically segment and determine the digital rock porosity, based on the OTSU's thresholding algorithm. In this work, twenty-two samples of 2D thin section petrographic image reservoir rocks of one Iraqi oil field are studied. The examples of thin section images are processed and digitized, utilizing MATLAB programming. In the present study, we have focused on determining of micro and macroporosity of the digital image. Also, some pore void characteristics, such as area and perimeter, were calculated. Digital 2D image analysis results are compared to laboratory core investigation results to determine the strength and restrictions of the digital image interpretation techniques. Thin microscopic image porosity determined using OTSU technique showed a moderate match with core porosity.

Keywords: Digital rock physics, OTSU thresholding, Thin section image, Porosity, Macro pores, Micro pores

Received on 26/06/2020, Accepted on 22/08/2020, published on 30/09/2020

<https://doi.org/10.31699/IJCPE.2020.3.8>

1- Introduction

Image analysis has been used for many years to extract relevant information from digital microscopic images. Image analysis includes all operations required to obtain quantified image information.

The typical image analysis sequence involves image acquisition, processing, segmentation, measurements, data processing and interpretation. Segmentation of images considers one of the essential techniques utilized to divide the image into its integrated portions for extracting the relevant image information [1].

Briefly, the segmentation of the image transforms the representation of an image into its simplified shape that can be examined more critically and naturally [2], [3].

Several practical image segmentation applications are available such as trace tumors and additional pathologies [4], [5], machine vision, object detection [6], face detection, medical imaging [7], [8], anatomic building studies and diagnoses [9], fingerprint recognition and video surveillance.

Several techniques of image segmentation, such as thresholding [10], edge-based segmentation [11], and compression-based methods [12], have been taken during recent decades.

In image processing techniques, many algorithms used, such as Artificial Neural Network [13], Convolutional Neural Network [14], and K - Nearest Neighbors. In all image segmentation methods, the simplest and most relevant and useful technique of dividing an image into the front class and the background class is thresholding technique [15].

The thresholding process converts the grayscale image into the binary image depending on the threshold values. The important of the thresholding process is to select an optimal threshold value when there are more threshold levels are implemented. Several methods of thresholding are currently employed, including OTSU technique, clustering [16] and utmost entropy technique [17].

OTSU method is fast and ease of coding thresholding method among all the purposes mentioned above.

Because the OTSU threshold operates on histograms (which are integer or float arrays of length 256) it's quite fast and approximately 90 lines MATLAB code needed.

However, OTSU technique is a histogram-based [18] threshold approach for automatic thresholding of the image. OTSU's algorithm suggests that the image can be divided into two main categories: foreground and background.

The algorithm designed to find the best threshold value that divides the histogram into two classes that maximizes the variance between two classes. The development of the current OTSU threshold to the multi-level threshold referred to as the multi-OTSU thresholds [19]. Porosity is the porous space fraction that the rock matrix does not occupy [20]. A comprehensive study of the distribution of porosity is essential for the reservoir evaluation project [21]. Porosity is a crucial property of rock due to measuring potential storage volume of hydrocarbons. In the carbonate reservoir, porosity ranges about 0.01-0.35 [22]. The volume fraction of void spaces, i.e. non-rock space, divided by the total volume of the sample defined as porosity [23]. High porosity values indicate high capacities of the reservoir rocks to contain these fluids, while low porosity values indicate the opposite [24].

The porosity evaluated either through formation evaluation logs or through laboratory measurements on core samples. A general industry practice is to regard core measurements as ground truth. However, there can be uncertainties associated with core measurements especially when laboratory conditions ignored under which core measurements were made.

There are certain factors that control porosity of a formation, pore and grain size distribution, mineralogy, sorting and diagenesis, etc. [25], [26]. Characterizing these controlling factors require advanced logging and special analysis on core data (SCAL), yet some of these properties require alternate interpretation techniques. 'Digital image analysis of thin sections' is presented as this alternate technique.

Porosity, mineralogy, pore size distribution and sorting analyzed through digital image analysis of thin sections. In this study, OTSU's thresholding implemented for microscopic image segmentation. The samples of microscopic images are processed utilizing MATLAB programming. In the present study, microporosity and macroporosity of the digital image are determined. Also, some pore void characteristics, such as area and perimeter, were calculated.

2- Material and Methods

In this work, twenty-two samples of 2D thin section petrographic image used for analyses from the core plugs taken from the Buzurgan oil field. Each sample was impregnated with blue-dyed epoxy, thin sectioned and then was stained for discrimination of carbonate minerals, the scanned image has resolution of about 10 μm/pixel.

The procedure of scanning and digitizing the image called 'optical microscopy' and is of lower resolution as compared to digital images obtained from 'scanning electron microscopy'. The advantage of the former is that it is a fast technique to obtain digital images and a disadvantage that pore sizes less than 10 μm cannot be quantitatively resolved with optical microscopy. In image processing, OTSU's technique used to implement automatic image thresholding, and this method named after Japanese scientist Nobuyuki OTSU [10].

The algorithm in the simplest form returns a single threshold of intensity to separate the pixels into two groups or classes, foreground and background. The algorithm searches deeply for the threshold that maximizes the variance of between-class or minimizes the variance of within-class.

The fundamental concept is that suitable threshold classes must separate the intensity values in terms of their pixel and, conversely, that the optimum threshold would be a threshold providing the best class separation in terms of intensity values [27].

OTSU's technique has the significant property, in relation to its optimality, that it is entirely based on computations executed on an image's histogram, an easily accessible 1-D array. Let {0, 1, 2 , L - 1} are the separate intensity levels in a digital image of size (M.N) (row and column dimensions of the image) pixels, and assume (n_i) is the number of pixels with intensity (i). The total image pixel is; $MN = n_0 + n_1 + n_2 + \dots + n_{L-1}$. the normalized histogram contains parts as [10];

$$p_i = \frac{n_i}{MN} \quad (1)$$

$$\sum_{i=0}^{L-1} p_i = 1 \text{ and } p_i \geq 0 \quad (2)$$

Where:

M.N = row and column dimensions of the image

n_i = the number of pixels with intensity (i)

P_i = probability distribution of intensity (i)

i = intensity

Now, assume that a threshold (T) was selected with value (0 < T < L-1), and utilized this threshold to separate the digital input image into two classes or groups, (C₁) and (C₂). Where (C₁) involves all the image pixels that have intensity values ranges (0, T) and (C₂) includes all the image pixels that have intensity values ranges (T+1, L-1). Utilizing this threshold, probability P₁(T) of class C₁ (i.e. Background class) is given by the cumulative sum;

$$P_1(T) = \sum_{i=0}^T p_i = \sum_{i=0}^T \frac{n_i}{MN} \quad (3)$$

Where: T = threshold.

In the same way, the probability of the second class P₂(T) (class C₂, or Foreground class) is given by;

$$P_2(T) = \sum_{i=T+1}^{L-1} p_i = 1 - P_1(T) \quad (4)$$

The class C₁ mean intensity value of the pixels is given by;

$$\mu_1(T) = \sum_{i=0}^T i p\left(\frac{i}{C_1}\right) = \sum_{i=0}^T i p\left(\frac{i}{i}\right) \left(\frac{P(i)}{P(C_1)}\right) = \frac{1}{P_1(T)} \sum_{i=0}^T i p_i \quad (5)$$

Where: μ₁(T) is mean intensity value for class C₁. Where P₁(T) is given in Eq. (2). The term $p\left(\frac{i}{C_1}\right)$ is the probability of value (i) which derives from class (C₁).

The second part of the Equation comes from Bayes' formula. The third part comes from the fact $p\left(\frac{C_1}{i}\right) = 1$, probability of (C1) for given (i) equal to (1), since only class (C₁) values is considered. While $P(i)$ is the probability of the (ith) value, which is simply the (ith) component of histogram(p_i). Finally, $P(C_1)$ is the probability of class (C₁) that is equal to Eq. (3). In the same way, the class (C₂) means intensity value of pixels given by;

$$\mu_2(T) = \sum_{i=T+1}^{L-1} i p\left(\frac{i}{C_2}\right) = \frac{1}{P_2(T)} \sum_{i=T+1}^{L-1} i p_i \quad (6)$$

Where: $\mu_2(T)$ is mean intensity value for class C₂. The term $p\left(\frac{i}{C_2}\right)$ is the probability of value (i) which derives from class (C₂).

The average intensity of the entire image (i.e., the *global mean*) given by;

$$\mu_G = \sum_{i=0}^{L-1} i p(i) \quad (7)$$

Where: μ_G = is a global mean or average intensity of the entire image

By substitute of the previous results, the validity of the following two equations can be confirmed:

$$P_1\mu_1 + P_2\mu_2 = \mu_G \quad (8)$$

And

$$P_1 + P_2 = 1 \quad (9)$$

Where:

P_1 = Background class (class C₁) probability.

P_2 = Foreground class (class C₂) probability.

μ_1 = mean intensity value for class C₁

μ_2 = mean intensity value for class C₂

μ_G = is a global mean or average intensity of the entire image

We can use the normalized, dimensionless metric to assess the "goodness" of the threshold at level (T)[28];

$$\eta = \frac{\sigma_B^2}{\sigma_G^2} \quad (10)$$

Where;

(σ_G^2) = *global variance* (the variance in intensity of all pixels in image)

η = dimensionless metric

(σ_B^2) = *between-class variance*

The global variance and it is given in Equation below [10];

$$\sigma_G^2 = \sum_{i=0}^{L-1} (i - \mu_G)^2 p_i \quad (11)$$

And *between-class variance* (σ_B^2) is given in Equation below;

$$\sigma_B^2 = P_1(\mu_1 - \mu_G)^2 + P_2(\mu_2 - \mu_G)^2 \quad (12)$$

Equation (12) can also be written as;

$$\sigma_B^2(T) = P_1 P_2 [\mu_1 - \mu_2]^2 \quad (13)$$

Eq. (13) showed that the σ_B^2 will be larger whenever the two means (μ_1) and (μ_2) are farther from each other, demonstrating that (*between-class variance*) separability measure between classes. Since (σ_G^2) is constant for a given image; therefore the (η) is a measure of separability also, and maximizing this dimensionless metric is equivalent to maximizing (σ_B^2) . Note that Eq. (10) assumes implicitly that $(\sigma_G^2 > 0)$. This variance can only be zero if all intensity levels in the image are the same, which implies that only one class of pixels exists. This, in turn, means that ($\eta = 0$) for a constant image since separability of single class from itself is zero. the final results yield when (T) reintroduced again:

$$\eta(T) = \frac{\sigma_B^2(T)}{\sigma_G^2} \quad (14)$$

And

$$\sigma_B^2(T) = P_1(T)[(\mu_1(T) - \mu_G)]^2 + P_2(T)[(\mu_2(T) - \mu_G)]^2 \quad (15)$$

Then, the best threshold value is the, (T*) that maximizes $\sigma_B^2(T)$:

$$\sigma_B^2(T^*) = \max_{0 \leq T \leq L-1} \sigma_B^2(T) \quad (16)$$

OTSU's algorithm also is defined as a weighted sum of the two classes' variances [10]:

$$\sigma_W^2 = P_1(T) \sigma_1^2(T) + P_2(T) \sigma_2^2(T) \quad (17)$$

Where: weights (P_1) and (P_2) are the probabilities of the background (class C1) and foreground(class C2) classes respectively, separated by a threshold (T) are stated previously. While $\sigma_1^2(T)$ is the variance of the pixels in the background (below threshold), $\sigma_2^2(T)$ is the variance of the pixels in the foreground (above threshold), given in Equations below;

$$\sigma_1^2(T) = \frac{1}{P_1(T)} \sum_{i=0}^T [i - \mu_1(T)]^2 p(i) \quad (18)$$

$$\sigma_2^2(T) = \frac{1}{P_2(T)} \sum_{i=T+1}^{L-1} [i - \mu_2(T)]^2 p(i) \quad (19)$$

And $\sigma_W^2(T)$ is *within-class variance*.

Then, the best threshold value is the, T* that minimizes $\sigma_B^2(T)$;

$$\sigma_W^2(T^*) = \min_{0 \leq T \leq L-1} \sigma_W^2(T) \quad (20)$$

For two classes, OTSU showed that minimizing the within-class variance is the same as maximizing within-class variance, in another meaning; subtracting within-class variance from the total variance get something called the between-class variance $\sigma_B^2(T)$ [29]. The best threshold using the OTSU method is the one maximizing overall between classes variance or minimizing overall within-class variance. In Fig. 1-a there is a simple bimodal distribution with two homogeneous classes where the threshold value (T) can be easily determined. If there is no valley one as shown in Fig. 1-b the method of determining threshold value (T) is minimizing the total variance within both classes or maximizes the overall variance between both classes. The best threshold is maximizing the between classes variance or, contrariwise, minimizing the within-class variance[30-31].

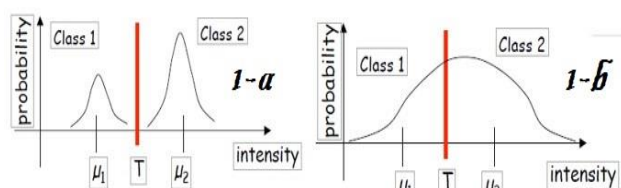


Fig. 1. Typical Image Histogram Show (1-a) Simple Bimodal Distribution (1-b) No-Bimodal Distribution

In this study, OTSU algorithm implementation started with converting the color image to grayscale image and plotting the input image's normalized histogram. According to the threshold value, the histogram pixels are separated into two clusters or class. The cumulative sums and the cumulative means for each class are calculated using Eq. (3) through (6). The total (global) intensity means it is calculated using Eq. (7). The between-class variance $\sigma_B^2(T)$ is calculated using Eq. (13), where the farther apart the means, the larger will be $\sigma_B^2(T)$. The maximum "between-class variance $\sigma_B^2(T)$ is set as an optimum OTSU threshold value (T*). When the maximum is not unique, the values corresponding to the detected maximum can be (T *) averaged. Finally, optimum separability measure, ($\eta *$) at (T = T*) is obtained using Eq. (14). The separability is a measure of how easily separable the classes are. A uniform distribution is (0), and a clear, bimodal is (1).

3- Calculations and Analysis

3.1. OTSU Thresholding Implementation

The objective of this section is to introduce and apply the binary segmentation algorithm of OTSU on the samples under study. MATLAB code created which automatically segment and determine the digital rock porosity, based on the OTSU's thresholding algorithm using the following main MATLAB code;

```
function level = otsu(histogramCounts)
total = sum(histogramCounts); % total number of pixels in the image
%% OTSU automatic thresholding
top = 256;
sumB = 0;
wB = 0;
maximum = 0.0;
sum1 = dot(0:top-1, histogramCounts);
for ii = 1:top
    wF = total - wB;
    if wB > 0 && wF > 0
        mF = (sum1 - sumB) / wF;
        val = wB * wF * ((sumB / wB) - mF) * ((sumB / wB) - mF);
        if ( val >= maximum )
            level = ii;
            maximum = val;
        end
    end
    wB = wB + histogramCounts(ii);
    sumB = sumB + (ii-1) * histogramCounts(ii);
end
end
```

As a first step, a pixel-value histogram using MATLAB image analysis toolbox plotted for each digital image, as shown in Fig. (2), because the used image type is an 8-bit image, there were (256) possible pixel values. The histogram height with 256 bins is calculated, where each bin's height is equal to the number of pixels with that pixel value from (0) to (255). For each given image, the probability of the pixel value (i) calculated using Eq. (3) by separating the height of bin by the complete number of pixels in the histogram. Since the goal is to maximize between-class variance, each class mean, global intensity means and variances of both classes calculated using Eq. (5), (7) and (15), respectively.

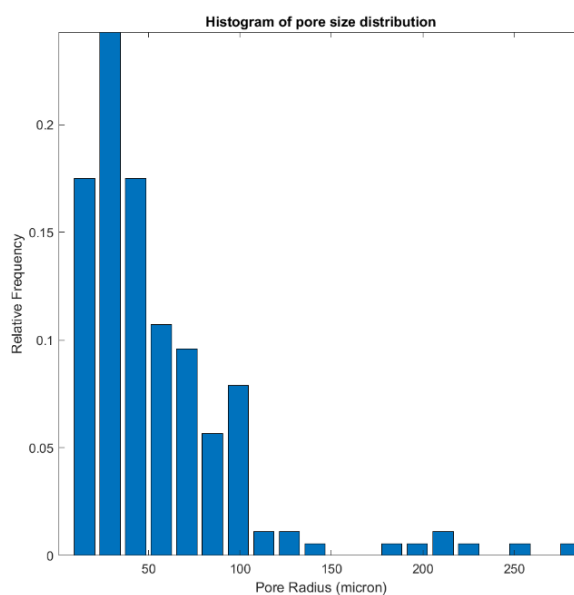


Fig. 2. Pixel-Value Image Histogram for Sample No.(7)

Finally, the OTSU threshold value (T_B) obtained as a value of for which $\sigma_B^2(T)$ is maximum. For not unique maximum threshold value, the OTSU threshold value (T_B) obtained by averaging the values of corresponding to the various maxima detected. Additionally, the separability measure, η^* was calculated using Eq. (14) at ($T = T_B$). It is sufficient to increase between class variance Eq. (13) this will decrease within-class variance too. Therefore, only the "between-class variance" calculated for each threshold and picked the threshold that maximizes the variance. Depending on each microscopic image quality, OTSU's algorithm was run several times for better results. The MATLAB function (*im2bw*) is used to convert an intensity image to a binary image. The binary image level which is a normalized intensity value that lies in the range (0, 1) was calculated depending on optimal threshold value (T_B). The results of threshold, class variance and separability criterion are for twenty-two used samples are listed in the Table 1. The results of OTSU thresholding are exposed in Fig. 3 for some analyzed samples, for example. It can be observed that the threshold of the OTSU has divided the digital image into two levels: white (porous) and Black (matrix) background.

3.2. Porosity and Pore Space Characteristics Determination

A digital image comprises pixels, which are building blocks of an image. Core samples image used in this study were cropped at (637x478) pixels; hence the total number of pixels in a sample is 304486 pixels. Core thin section samples consist of empty pore space filled with the blue liquid epoxy and solid grains comprising of different minerals colors, as shown in Fig. 3. The definition of porosity from image analysis can be written in pixels term as [32-33];

$$Porosity (Image) = \frac{\sum \text{pixels in pore space}}{\text{Total number of pixels}} \quad (21)$$

Table 1. Results of OTSU Thresholding Method Parameters

CoreID	Threshold	Separability Criterion	Between Class Variance	Level	Global Mean
7	116	0.738	2014.095	0.453	77.549
19	70	0.655	857.701	0.273	51.699
23	82	0.673	977.849	0.32	60.731
24	98	0.651	352.521	0.383	99.982
25	130	0.6607	1290.457	0.508	108.541
27	60	0.692	901.321	0.234	31.857
30	63	0.642	843.274	0.246	47.497
31	79	0.665	1249.349	0.309	51.538
35	94	0.797	1968.251	0.367	52.731
36	83	0.751	1673.708	0.324	55.031
37	108	0.794	2587.521	0.422	58.826
38	67	0.621	615.282	0.262	49.961
39	117	0.814	2494.852	0.457	60.336
45	65	0.614	628.847	0.254	47.842
46	79	0.639	652.216	0.309	48.881
47	82	0.640	1128.102	0.32	48.569
48	55	0.604	280.360	0.215	35.338
49	113	0.838	2917.877	0.441	56.905
50	109	0.473	321.355	0.426	108.324
51	71	0.617	564.410	0.277	52.768
52	67	0.620	554.612	0.262	42.295
53	64	0.5693	443.973	0.25	40.040

Porosity also defined in terms of pore sizes as micro and macropores. Core thin section samples used in the current study were scanned with optical microscopy having a pixel resolution of (10 μm).

Substantial porosity may be residing in pore sizes less than (10 μm), i.e. sub-resolution pores. Such sub-resolution pores were visually observe-able on thin-section images but with a mixed response of clay-silt matrix and porosity.

In the current study, sub-resolution pores are defined as (Micro Pores), and pore sizes larger than (10 μm) is defined as (Macro Pores). A subjective adjustment factor was used to extract matrix effect from sub-resolution pores as [25];

$$\varphi_{image} = A * \varphi_{micro} + \varphi_{macro} = \varphi_{total} \quad (22)$$

Where:

φ_{image} = porosity derived from image analysis

φ_{micro} = microporosity derived from image analysis

φ_{macro} = macroporosity derived from image analysis

φ_{total} = total porosity derived from image analysis

Ain = adjustment factor (between 0 and 1) to remove matrix effect from sub-resolution pores.

As a pixel representing pore size of less than 10 μm may consist of *both* a grain and a pore. Φ_{micro} is micro pores porosity, and Φ_{macro} is macro pores porosity. Microporosity was adjusted by the factor ($A = 0.75$) to exclude matrix effect from micropores, and image porosity is calculated using Equation (22).

The results of image porosity obtained by OTSU's thresholding techniques are listed in the Table 2 with the comparison with core porosity. Fig. 4 shows a comparison of porosity obtained OTSU's thresholding techniques vs core porosity. The task of digital rock analysis needs to be quantitatively measured in an area of interest, whether it is pores or grains, extracted from a digital rock image.

The extracted objects are binary objects, where interest object with object label map is presented. Binary objects characteristically interpreted to get a value of (1), and the residual pixels to reach a value of (0). A binary object can be described by size, shape or distance from other objects. An object's size can be defined by area and perimeter.

The area is a suitable measure of the total size. Perimeter is mainly ideal for discriminating between objects with simple shapes and those with complex shapes. Consider the function $I_n(i, j)$ described for the object of an (MxN) image:

$$I_n(i, j) = \begin{cases} 1 & \text{if } I(i, j) = n^{th} \text{ object number} \\ 0 & \text{otherwise} \end{cases} \quad (23)$$

The area in pixels is then specified by;

$$A_n = \sum_{i=0}^{M-1} \sum_{j=0}^{N-1} I_n(i, j) \quad (25)$$

The simple calculation of the perimeter takes from the number of boundary pixels belonging to an object. This achieved thru calculating pixels number with a value of (1) and at least one adjacent pixel of (0).

Another problem in the measurement of the perimeter is to separate an object's internal and external perimeter (segmented pores).

The boundary pixel exact vertex points usually understood to be at the center of that pixel. The boundary pixels location for perimeter measurement yields internal perimeter; external perimeter yields with the boundary of pixels in the background around the object; as shown in Fig. 5.

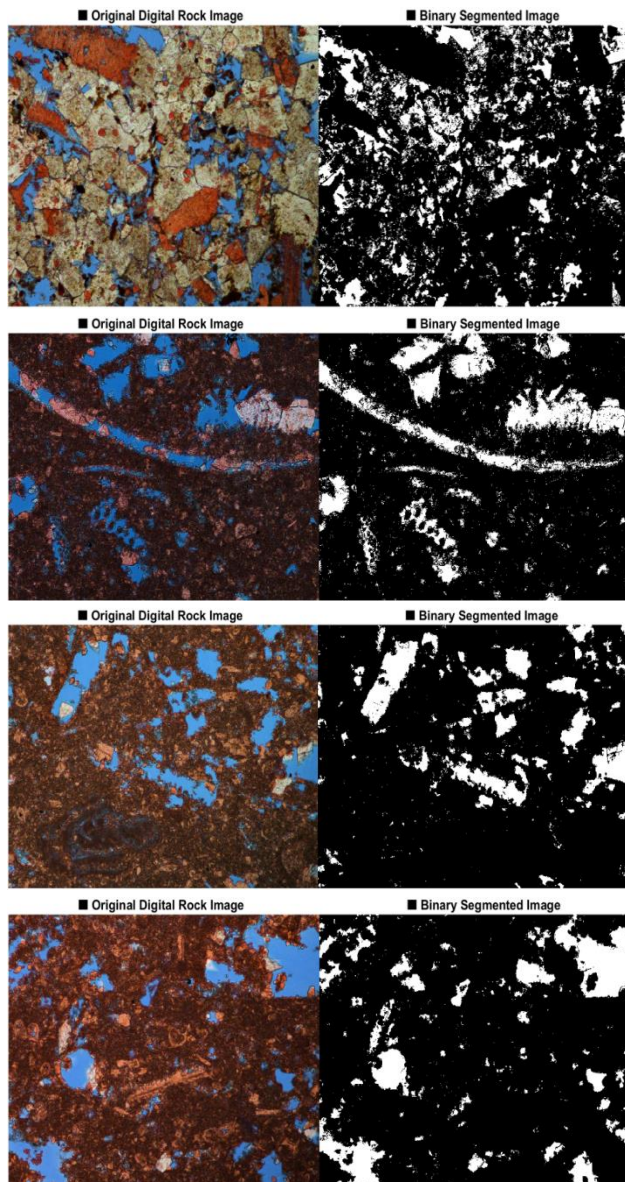


Fig. 3. Original and Segmented Binary Rock Images Thresholds Using OTSU Method (Samples 25,35,39, and 49 respectively from top to bottom)

Table 2. Image porosity analysis results using the OTSU thresholding method

Core ID	total pores	macropores	micropores	Phi_Macro	Phi_Micro	PHI_Im	PHI_Core
7	304486	41837	9137	0.137	0.030	0.159	0.182
19	304486	29577	30561	0.097	0.100	0.172	0.193
23	304486	33739	8747	0.110	0.028	0.132	0.145
24	304486	22551	8474	0.074	0.027	0.094	0.095
25	304486	36559	9924	0.120	0.032	0.144	0.158
27	304486	14852	13283	0.048	0.043	0.081	0.085
30	304486	48714	14699	0.159	0.048	0.196	0.207
31	304486	40496	16749	0.132	0.055	0.174	0.199
35	304486	33036	6687	0.108	0.021	0.124	0.142
36	304486	35322	9609	0.116	0.031	0.139	0.144
37	304486	42083	3843	0.138	0.012	0.147	0.184
38	304486	47138	15888	0.154	0.052	0.193	0.212
39	304486	50218	12294	0.164	0.040	0.195	0.217
45	304486	48565	13666	0.159	0.044	0.193	0.213
46	304486	21743	13485	0.071	0.044	0.104	0.147
47	304486	17129	27177	0.056	0.089	0.123	0.147
48	304486	18437	15278	0.060	0.050	0.098	0.17
49	304486	38680	3195	0.127	0.010	0.134	0.167
50	304486	13801	9660	0.045	0.031	0.069	0.12
51	304486	25996	13299	0.085	0.043	0.118	0.128
52	304486	28605	12458	0.093	0.040	0.124	0.139
53	304486	21650	14724	0.071	0.048	0.107	0.156

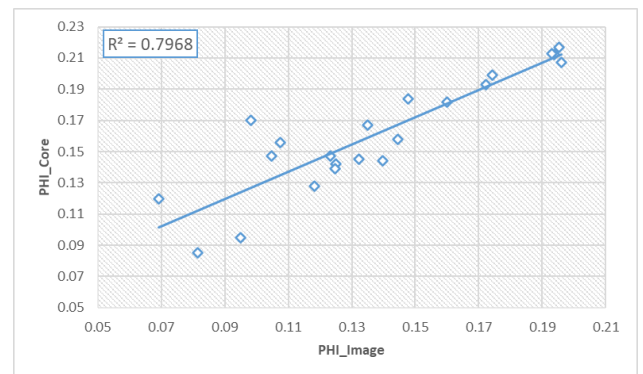


Fig. 4. Comparison of image-based total porosity using OTSU thresholding method with core porosity

The circular equivalent diameter defined as the diameter of a circle with the same area as the region. Thus, once the area of the pore measured, the equivalent diameter (D_{eq}) calculated as [26];

$$D_{eq} = \sqrt{\frac{4A}{\pi}} \tag{25}$$

Specific surface area or surface to volume ratio is approximated by the ratio of pore perimeter to pore area. Perimeter and area of each pore (i) are outputs of binary image analysis as discussed previously. The specific surface area of digital binary rock sample image is written as [26];

$$S_i = \frac{\text{Pore Perimeter}}{\text{Pore Area}} \quad (26)$$

The specific area of the analyzed sample is approximated as the average specific area of all pores.

$$s = \frac{1}{N} \sum S_i \quad (27)$$

The results of image pore space characteristics obtained by OTSU's thresholding techniques are listed in the table (3).

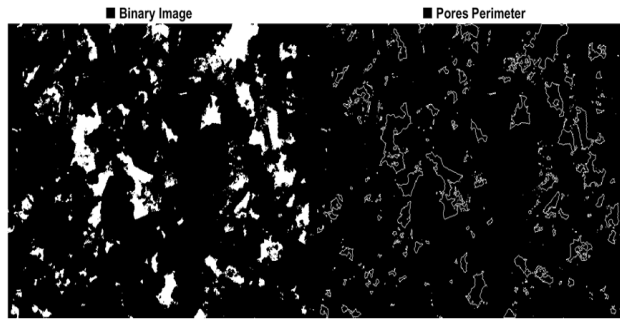


Fig. 5. Perimeter measurement by counting the number of object boundary pixels

Table 3. Image pore space characteristics results using OTSU thresholding method

Core ID	Avg. Area (μm^2)	Avg. Equiv. Diameter (μm)	Avg. Perimeter (μm)	Avg. Specific surface area ($1/\mu\text{m}$)
7	49.45	3.774	18.355	1.088
19	10.911	2.659	10.927	1.2691
23	31.01	3.412	18.228	1.178
24	28.788	3.754	17.583	1.136
25	42.531	4.403	22.288	1.092
27	25.809	3.131	12.076	1.064
30	32.995	3.413	18.412	1.111
31	24.72	3.364	14.549	1.1028
35	51.983	3.489	19.649	1.201
36	44.861	3.172	15.724	1.185
37	92.241	4.973	26.83	1.077
38	29.816	3.443	17.315	1.140
39	102.234	5.658	27.138	1.009
45	35.332	3.436	18.804	1.169
46	21.252	3.390	13.455	1.137
47	7.144	2.165	6.754	1.249
48	15.916	3.061	11.361	1.138
49	116.055	5.648	26.785	1.004
50	23.206	3.619	14.817	1.101
51	18.550	3.139	13.178	1.181
52	26.980	3.474	15.193	1.134
53	19.365	3.190	12.951	1.1583

3.3. Results and Discussion

In this study, three statistical parameters are considered for the analysis of image porosity resulted from a digital image.

These statistical parameters utilized to assess the accuracy of porosity predicted from the digital rock analysis. Absolute average percent relative error (AARE) used to quantify the average value of the absolute relative deviation of measured porosity value from experimental core porosity data.

The standard deviation of the estimated image porosity relative to the experimental values is essential to measure the accuracy of the correlation and used algorithm. The value of standard deviation is usually expressed in percent, and the small value indicates higher accuracy.

The purpose of performing the correlation coefficient is to describe the strength of the association between two variables, namely experimental and calculated values.

The correlation coefficient (R) expresses the presence or non-presence of a linear interrelationship between the two observed variables. If the linear interrelationship is positive, the correlation coefficient will be a positive number between 0 and 1.0. If, on the other hand, it is negative, the number will be between (0) and (1).

The coefficient of determination (R^2) is the square of the coefficient of correlation (R) shows percentage variation in the y-axis that described by all x-axis variables collected. It is varied between (0) and (1) with higher values is better. The results of AARE, standard deviation, correlation coefficient, and coefficient of determination are 14.66, 0.029, 0.892 and 0.796, respectively.

4- Discussions and Conclusions

Porosity from image analysis was compared against core porosity to validate the goodness of porosity prediction from image analysis. However, uncertainties associated with both measurements shall be considered as well. Porosity from image analysis is limited to pixels resolution of optical microscopy and represents a very small section of the rock sample.

Core porosity is determined on the 1-inch cylindrical plug while the dimensions of thin section sample are only 35 μm thick with a diameter of 1-inch.

The volume investigated is different. Studied scanned samples with optical microscopy had a pixel resolution of 10 μm . Pore sizes larger than (10 μm) (i.e. macropores) were correctly resolved, but there was a significant quantity of sub-resolution pores (micropores) with mixed response of pore and matrix.

A subjective adjustment factor used to take out this matrix effect from micro-pores. This single value of adjustment factor was determined while comparing image porosity against core porosity for all samples. This factor has selected as (0.75) in this study to correct the matrix effect during OTSU segmentation method.

The suggested value may have worked for the analyzed samples of the current research and can differ in other environments. Uncertainty analysis can also be analyzed for porosity from thin section image analysis.

As follows from error analysis results, due to an appropriate choice and capture of blue color using OTSU algorithm segmentation, the porosity obtained by image analysis is quite close to the core porosity. The errors are about 14.66% with a standard deviation of about 0.029 and high correlation coefficient of ($R = 0.892$). Furthermore, binary images capture the pore distribution excellently without counting matrix material as pore space.

Digital thin section image analysis can be considered as an alternate technique to evaluate porosity and pore space rock properties rather than experimental core analysis. Histogram thresholding established method had the element of subjectivity in it where the threshold on pixel intensity histogram had to be manually adjusted till the analyst is visually satisfied that pore space adequately captured.

This visual analysis was challenging, as optically scanned images used in the current study had a pixel resolution of $10\mu\text{m}/\text{pixel}$, and there were a significant number of pores with size less than the pixel resolution. In another study, regression equations used to achieve a good correlation of porosity between image analysis and routine core analysis data.

These adjustments and regression lost the predictive power of image analysis. OTSU clustering introduced as an automatic technique to separate the intensity histogram into two parts and segment the pores from the matrix. Thin sections image porosity using the OTSU technique showed a good match with core porosity; with the additional benefit, that workflow now automated. Moreover, the OTSU method can predict threshold values if it desired to make image interpretation with a thresholding technique. In the current study, porosity is the main petro physical property determined from thin section images. For future work, the permeability as a function of porosity and pore space characteristics can be estimated.

The predictive power of the OTSU method is encouraging, as it can be applied on vastly available drill cuttings as a secondary means of porosity data. However, for the wells where conventional core data is not available or possible, porosity can be determined from thin section images for its integration with well logs interpretation to reduce uncertainties. Some limitations to thin section image analysis were also observed. For optically scanned images, pore sizes less than $10\mu\text{m}$ had a mixed response of matrix and porosity.

A subjective but a single adjustment factor was required to remove the matrix effect from such pores for all analyzed samples.

This is equally applicable for both automatic and manual thresholding techniques. Clustering analyzes porosity from pore filling blue epoxy, i.e., a blue cluster; it was observed that clustering over-estimates porosity if blue color is also present as a matrix color. Such a situation will be equally challenging for manual thresholding and hence, can be concluded as a general limitation of thin section image analysis.

References

- [1] [R. C. Gonzalez and R. E. Woods, Digital image processing. New Jersey: Parson, 2008.](#)
- [2] L. G. Shapiro and G. C. Stockman, "Computer Vision. 279-325," ed: New Jersey, Prentice-Hall, ISBN 0-13-030796-3, 2001.
- [3] [L. Barghout and L. Lee, "Perceptual information processing system." U.S. Patent Application 10/618,543, filed March 25, 2004.](#)
- [4] [P. Shanthakumar and P. Ganesh Kumar, "Computer aided brain tumor detection system using watershed segmentation techniques", International Journal of Imaging Systems and Technology, vol. 25, no. 4, pp. 297-301, 2015.](#)
- [5] [E. B. George and M. Karnan, "MR brain image segmentation using bacteria foraging optimization algorithm," International journal of engineering and technology \(IJET\), vol. 4, pp. 295-301, 2012.](#)
- [6] [J. Delmerico, P. David and J. Corso, "Building facade detection, segmentation, and parameter estimation for mobile robot stereo vision", Image and Vision Computing, vol. 31, no. 11, pp. 1632-1639, 2013.](#)
- [7] [D. L. Pham, et al., "Current methods in medical image segmentation," Annual review of biomedical engineering, vol. 2, pp. 315-337, 2000.](#)
- [8] [M. Forouzanfar, N. Forghani and M. Teshnehlab, "Parameter optimization of improved fuzzy c-means clustering algorithm for brain MR image segmentation", Engineering Applications of Artificial Intelligence, vol. 23, no. 2, pp. 160-168, 2010.](#)
- [9] [S. Kamalakannan, "Double-edge detection of radiographic lumbar vertebrae images using pressurized open DGVF snakes," IEEE Transactions on Biomedical Engineering, vol. 57, pp. 1325-1334, 2010.](#)
- [10] [N. Otsu, "A Threshold Selection Method from Gray-Level Histograms", IEEE Transactions on Systems, Man, and Cybernetics, vol. 9, no. 1, pp. 62-66, 1979.](#)
- [11] [O. Wirjadi, "Survey of 3d image segmentation methods," 2007.](#)
- [12] [H. Mobahi, S. Rao, A. Yang, S. Sastry and Y. Ma, "Segmentation of Natural Images by Texture and Boundary Compression", International Journal of Computer Vision, vol. 95, no. 1, pp. 86-98, 2011.](#)
- [13] [Md. Abu Bakr Siddique, Mohammad Mahmudur Rahman Khan, Rezoana Bente Arif and Zahidun Ashrafi, "Study and observation of the variations of accuracies for handwritten digits recognition with various hidden layers and epochs using neural network algorithm." In 2018 4th International Conference on Electrical Engineering and Information & Communication Technology \(iCEEICT\), pp. 118-123. IEEE, 2018.](#)

- [14] [Rezoana Bente Arif, Md. Abu Bakr Siddique, Mohammad Mahmudur Rahman Khan and Mahjabin Rahman Oishe, "Study and Observation of the Variations of Accuracies for Handwritten Digits Recognition with Various Hidden Layers and Epochs using Convolutional Neural Network." In 2018 4th International Conference on Electrical Engineering and Information & Communication Technology \(iCEEICT\), pp. 112-117. IEEE, 2018.](#)
- [15] [Mohammad Mahmudur Rahman Khan, Rezoana Bente Arif, Md. Abu Bakr Siddique and Mahjabin Rahman Oishe, "Study and Observation of the Variation of Accuracies of KNN, SVM, LMNN, ENN Algorithms on Eleven Different Datasets from UCI Machine Learning Repository", in 2018 4th International Conference on Electrical Engineering and Information & Communication Technology \(IEEE ICT\), 2018, pp. 124-129.](#)
- [16] [M. Sezgin and B. Sankur, "Survey over image thresholding techniques and quantitative performance evaluation", Journal of Electronic Imaging, vol. 13, no. 1, pp. 146-166, 2004.](#)
- [17] [Y. Zhang and L. Wu, "Optimal multi-level thresholding based on maximum Tsallis entropy via an artificial bee colony approach," Entropy, vol. 13, pp. 841-859, 2011.](#)
- [18] [A. dos Anjos and H. Shahbazkia, "Bi-Level Image Thresholding-A Fast Method", in BIOSIGNALS \(2\), 2008, pp. 70-76.](#)
- [19] [P.-S. Liao, "A fast algorithm for multi-level thresholding," J. Inf. Sci. Eng., vol. 17, 2001, pp. 713-727.](#)
- [20] [Ghassan H. Ali, Yahya J. Tawfeeq, and Mohammed Y. Najmuldeen, "Comparative estimation of water saturation in a carbonate reservoir: A case study of northern Iraq", Periodicals of Engineering and Natural Sciences, nol. 7, No. 4, pp.1743-1754, 2019.](#)
- [21] [Mohammed Y. Najmuldeen, Ali A. Fadhil, and Yahya J. Tawfeeq, "Petrophysical Characterization of The Tertiary Oil Reservoir, Northern Iraq", Periodicals of Engineering and Natural Sciences, ISSN 2303-4521, Vol. 8, No. 2, 2020.](#)
- [22] [Karrar Hayder Jassim and Jalal A. Al-Sudani, " Re-evaluation of Petro physical Properties in Yammama Formation at Nasiriya Field". Iraqi Journal of Chemical and Petroleum Engineering, Vol.20 No.3, 2019, pp. 59 – 66.](#)
- [23] [Yahya J. Tawfeeq, Mohammed Y. Najmuldeen and Ghassan H. Ali, "Optimal statistical method to predict subsurface formation permeability depending on open hole wireline logging data: A comparative study", Periodicals of Engineering and Natural Sciences, ISSN 2303-4521, Vol. 8, No. 2, 2020.](#)
- [24] [Sara S. Zughar, Ahmad A. Ramadhan, Ahmed K. Jaber, "Petrophysical Properties of an Iraqi Carbonate Reservoir Using Well Log Evaluation," Iraqi Journal of Chemical and Petroleum Engineering, vol.21, no.1, pp. 53 – 59,2020.](#)
- [25] [Fens, T.W., "Petrophysical properties from small rock samples using image analysis techniques", Ph.D, Delft University of Technology, 2000.](#)
- [26] [Zerabruk, B.T., Nermoen, A., Nadeau, P.H., "Digital image analysis for petrophysical characterization", M.Sc., University of Stavanger, 2017.](#)
- [27] [Sonka, Hlavac and Boyle, "Digital Image Processing and Computer Vision", India Edition, CENGAGE Learning, 2007.](#)
- [28] [K. Fukunaga, Introduction to statistical pattern recognition. Elsevier, 2013. pp. 260-267.](#)
- [29] [J. Gong, L. Li, and W. Chen, "Fast recursive algorithms for two-dimensional Thresholding," Pattern Recognition, vol. 31, no. 3, pp. 295–300, 1998.](#)
- [30] [Zhang, Jun and Hu Jinglu, "Image segmentation based on 2D Otsu method with histogram analysis", Computer Science and Software Engineering, 2008 International Conference on. 6: 105–108.](#)
- [31] [Zhu, Ningbo and Wang, Gang and Yang, Gaobo and Dai, Weiming, "A fast 2d otsu thresholding algorithm based on improved histogram", Pattern Recognition, 2009. CCPR 2009, Chinese Conference on: 1–5.](#)
- [32] [Varfolomeev, I., Yakimchuk, I., Denisenko, A., Khasanov, I., Osinceva, N., Rahmattulina, A., "Integrated study of thin sections: Optical petrography and electron microscopy", SPE 182071, 2016.](#)
- [33] [Lawrence, M., Jiang, Y., "Porosity, pore size distribution, micro-structure." In Bio-aggregates based building materials, pp. 39-71. Springer, Dordrecht, 2017](#)

تحليل مسامية النماذج الصخرية الرقمية بالاستناد على تقنية عتبة OTSU باستخدام الماتلاب

يحيى جرجيس توفيق وجمال عبد الواحد السوداني

قسم هندسة النفط، كلية الهندسة، جامعة بغداد، بغداد، العراق

الخلاصة

تلعب المسامية دوراً أساسياً في الجيولوجيا وهندسة البترول. وهي تتحكم في تخزين السوائل في طبقات المياه الجوفية وحقول النفط والغاز وتوصيل هيكل المسام للتحكم في تدفق السوائل وانتقالها من خلال تكوينات الخزان. لتحديد العلاقات بين المسامية والتخزين والنقل وخصائص الصخور، يجب قياس بنية المسام ووصفها كمياً. حساب مسامية الصور الرقمية باستخدام معالجة الصور يعد امراً مهماً لتحليل صخور المكامن حيث يتم فيها وصف المسامية ثنائية الأبعاد للعينة. العمليات الوثنائية يستخدم عملية تحويل الصورة الى ابيض واسود حيث تستخدم حد قيمة البيكسل لتحويل الصور الملونة والرمادية إلى صور ثنائية. والفكرة هي استيعاب المناطق الزرقاء بالكامل مع المسام وتحويلها إلى اللون الأبيض في صورة ثنائية ناتجة. تقدم هذه الدراسة إمكانات استخدام معالجة الصور لتحديد مسامية عينات الصخور الرقمية ثنائية الأبعاد في صخور مكامن الكربونية. تم إنشاء كود ماتلاب، والذي يقوم تلقائياً بتقطيع مسامية الصخور الرقمية وتحديدتها، استناداً إلى خوارزمية عتبة OTSU. في هذا العمل، تمت دراسة 22 عينة من صخور مكمن الصورة ذات مقطع رقيق ثنائي الأبعاد لحقل نفط عراقي. تتم معالجة أمثلة صور القسم الرقيق ورقمنتها باستخدام برمجة ماتلاب. في الدراسة الحالية، ركزنا على حساب مسامات المايكرو والماكرو للصورة الرقمية. أيضاً، تم حساب بعض خصائص الفراغ المسامي، مثل الحجم والمحيط. تم مقارنة نتائج تحليل الصور الرقمية ثنائية الأبعاد بنتائج المسامية من الفحص المختبري لتحديد قوة تقنيات تفسير الصور الرقمية المستخدمة. أظهرت مسامية الصورة الدقيقة المجهرية التي تم حسابها باستخدام تقنية OTSU تطابقاً جيداً مع المسامية المحسوبة من الفحوصات المختبرية.

الكلمات الدالة: فيزياء الصخور الرقمية، عتبة أوتسو، صورة المقطع الرقيق، المسامية، مسامات المايكرو، مسامات الماكرو.